Assimilation of wind speed and direction observations: results from real observation experiments

Feng Gao, Xiang-Yu Huang, Neil A. Jacobs & Hongli Wang

Assimilation of wind speed and direction observations: results from real observation experiments

By FENG GAO[1]*, XIANG-YU HUANG[2], NEIL A. JACOBS[3] and
HONGLI WANG[4,5], [1]*National Center for Atmospheric Research, Boulder, CO, USA*; [2]*Centre for Climate Research Singapore, Meteorological Service Singapore, Singapore*; [3]*Panasonic Avionics Corporation, Morrisville, NC, USA*; [4]*Cooperative Institute for Research in the Atmosphere, Colorado State University, Fort Collins, CO, USA*; [5]*Global Systems Division, National Oceanic and Atmospheric Administration/Earth System Research Laboratory, Boulder, CO, USA*

ABSTRACT

The assimilation of wind observations in the form of speed and direction (asm_sd) by the Weather Research and Forecasting Model Data Assimilation System (WRFDA) was performed using real data and employing a series of cycling assimilation experiments for a 2-week period, as a follow-up for an idealised post hoc assimilation experiment. The satellite-derived Atmospheric Motion Vectors (AMV) and surface dataset in Meteorological Assimilation Data Ingest System (MADIS) were assimilated. This new method takes into account the observation errors of both wind speed (*spd*) and direction (*dir*), and WRFDA background quality control (BKG-QC) influences the choice of wind observations, due to data conversions between (*u,v*) and (*spd, dir*). The impacts of BKG-QC, as well as the new method, on the wind analysis were analysed separately. Because the *dir* observational errors produced by different platforms are not known or tuned well in WRFDA, a practical method, which uses similar assimilation weights in comparative trials, was employed to estimate the *spd* and *dir* observation errors. The asm_sd produces positive impacts on analyses and short-range forecasts of *spd* and *dir* with smaller root-mean-square errors than the *u,v*-based system. The bias of *spd* analysis decreases by 54.8%. These improvements result partly from BKG-QC screening of *spd* and *dir* observations in a direct way, but mainly from the independent impact of *spd* (*dir*) data assimilation on *spd* (*dir*) analysis, which is the primary distinction from the standard WRFDA method. The potential impacts of asm_sd on precipitation forecasts were evaluated. Results demonstrate that the asm_sd is able to indirectly improve the precipitation forecasts by improving the prediction accuracies of key wind-related factors leading to precipitation (e.g. warm moist advection and frontogenesis).

Keywords: WRFDA, observation operator, observation error, quality control, variational assimilation

1. Introduction

Many types of platforms measure winds, such as surface land and marine observation networks, upper-air observation networks, aircraft and remote sensing systems. Generally, wind speed (*spd*) and direction (*dir*) are the initial products; however, the nature of wind vector measurements varies among these platforms. For example, surface winds (*spd* and *dir*) are typically measured by an anemometer on a fixed or drifting platform by a defined time-average.[1] For

aircraft-based observations, *spd* and *dir* are computed by taking the difference between the ground track vector,[2] which includes a Global Position System (GPS)-observed speed and angle based on the latitude and longitude change between adjacent points, and the aircraft track vector, which is derived from the true air speed[3] and the internal navigation system heading (Painting, 2003; Gao et al., 2012). Atmospheric Motion Vectors (AMV), in the forms of *spd* and *dir*, are derived from satellite imagery by tracking features over a sequence of images (Velden

---

[2]Horizontal speed in which the aircraft moves relative to a fixed point on the ground.
[3]Speed in which the aircraft moves relative to the surrounding air.

1

et al., 1998; NOAA Technical Report[4]; EUMETSAT report[5]).

The standard Weather Research and Forecasting Model Data Assimilation System (WRFDA) assimilates wind observations in the form of longitudinal and latitudinal components, conventionally abbreviated to u and v (asm_uv), which are computed from the initial observation product of spd and dir (Huang et al., 2009; Barker et al., 2012). This method is similar to other data assimilation systems, such as those described by Le Dimet and Talagrand (1986), Andersson et al. (1998) and Gustafsson et al. (2001).

In asm_uv, during the observation processing phase, which precedes assimilation, only the observational error associated with spd is used to quantify errors in u and v (Kalnay et al., 1996; Lindskog et al., 2001). This process allows the background quality control (BKG-QC) to proceed, thereby screening observations and computing a cost function based on the assimilation weight for wind-related terms.

However, the dir observational error, which can contribute uncertainty to u and v, is typically ignored. In fact, a nonlinear relationship exists between the observational errors of u and v and the errors in spd and dir. As eqs. (16) and (17) in Huang et al. (2013) indicate, the impact of dir observational error on the errors in u and v is both significant and sensitive to the background. As a result, dir observational error should not be ignored in wind data assimilation.

A new assimilation method for wind observations, which employs direct assimilation of spd and dir (asm_sd), has been developed for WRFDA (Huang et al., 2013). This method considers the dir observational error as being independent of the spd observational error, and thus the corresponding weights of spd or dir observations in the analysis are affected exclusively by the respective spd or dir observational errors.

Because it is not straightforward to build equivalent relationships among the wind measurement errors expressed in each format (Euclidean vs. radial) and the background errors of stream function/velocity potential, it is inaccurate to assume that asm_uv and asm_sd are equivalent in terms of assimilation variables due to the accuracy of transforming u and v from spd and dir. Additionally, the BKG-QC routine determines which wind observations to retain in different ways in asm_uv versus asm_sd, such that the accepted observations could vary even when the same dataset is used.

Distinct differences exist for the assimilation methods for spd and dir. In asm_sd, the spd (dir) observation and its error have an independent impact on the spd (dir) analysis. By comparison, the spd analysis is also affected by dir observations in addition to the spd observations in asm_uv. In other words, the spd analysis varies with the dir observation when the spd observation and the observational errors of u and v are constant in asm_uv, and the opposite is true for dir. These distinctions are responsible for generating different wind analyses in asm_uv compared to asm_sd.

Three key factors highlight the advantages of asm_sd real experiments:

(1) BKG-QC is able to screen spd or dir observations out separately in a direct way in asm_sd. This is an advantage because there is not an effective mechanism to guarantee that u and v components computed from a spd or dir observations, that can have substantial errors, will be screened out in asm_uv.

(2) The formulation of asm_sd ensures that the spd and dir analysis falls between the background and observations for both variables. In asm_uv, when u or v components point in opposite directions to the background, the asm_uv could produce a spd analysis with magnitude much smaller than what it should be. An extreme case could result in a spd of zero in the analysis regardless of spd in the background and observations (Fig. 1).

(3) Unlike most surface observation stations that independently observe spd and dir, AMV and aircraft-based wind measurements are calculated from vector differences, which could lead to error correlation between dir and spd. Regardless, it is more accurate to assume that the spd observational error is independent from the dir error than to assume the same for u and v because observation error in either spd or dir affects the observational errors of both u and v simultaneously. This assumption, widely used in this type of work (e.g. Hollingsworth and Lönnberg, 1986), simplifies the observation error covariance matrix to a diagonal matrix and is more acceptable in three dimensional variational data assimilation (3D-Var) versus 4D-Var, where some successive reports from the same station could be assimilated (Jarvinen et al., 1999).

Initial comparisons between asm_uv and asm_sd by using simplified arguments and graphical illustrations were conducted by Huang et al. (2013). Although the superiority of asm_sd was demonstrated by Observation System Experiments (OSEs), the forecast model was assumed to be error free, and the 'true' observational errors of spd and dir were
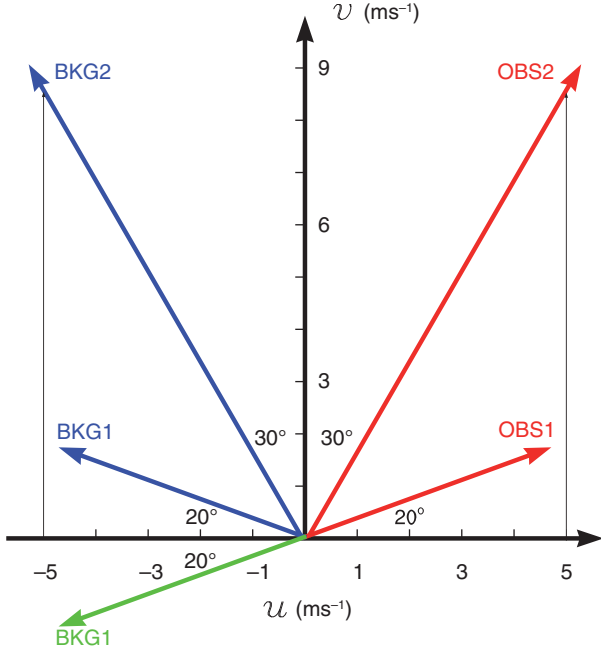
Fig. 1. Diagram of background wind vectors (BKG1 and BKG2) and the observational wind vectors (OBS1 and OBS2), used to present the differences of WRFDA background quality control procedures (BKG-QC) between asm_uv (standard assimilation method in WRFDA, assimilating wind observation in the forms of *u* and *v* components) and asm_sd (new assimilation method, assimilating wind observation in the forms of wind speed and direction).

predefined instead of truly known. Additionally, observations were assimilated without any quality control. Unfortunately, none of these assumptions and conditions are valid for any experiment using real data. While this topic has never been directly addressed, the issue of estimating *spd* and *dir* observational error in relation to the BKG-QC procedures has previously been raised: how should *spd* and *dir* observation errors be calculated in practice?

Several studies suggest comparing an observation with an uncorrelated reference. Benjamin et al. (1999) reported on a collocation study for Aircraft Communications Addressing and Reporting System (ACARS) observations generated from aircraft with different tail numbers. Likewise, Drüe et al. (2008) estimated the observation errors of Aircraft Meteorological Data Relay (AMDAR) by considering rawinsonde observations (RAOB) as the reference. With Tropospheric Airborne Meteorological Data Reporting (TAMDAR) becoming an important part in the global observing system, Moninger et al. (2010) presented error characteristics of TAMDAR by comparing them with the Rapid Update Cycle (RUC) 1-h forecast. Although strict collocation conditions were used, these estimations actually only provide an upper bound on the combined errors of observation, reference and representativeness.

Meanwhile, the variable *dir* is not involved in these studies. Gao et al. (2012) calculated *spd* and *dir* observational error, independent from any reference, of TAMDAR and RAOB by matching up three types of data sources. This method is theoretically suitable for any observation type; however, it is difficult to implement that method because no other available data type has sufficient coverage to co-locate with surface data over the continental United States (CONUS). Consequently, a practical method is employed in this study to estimate the *spd* and *dir* observation errors, which are used to obtain similar assimilation weights for wind observations in asm_uv and asm_sd, as in the initial test.

Since *dir* observations can be screened out directly by BKG-QC in asm_sd, it is necessary and reasonable to define a critical value of *dir* innovation to decrease the possibility of absorbing *dir* observations that are grossly in error. Some studies have demonstrated that a large *dir* error is often correlated to light *spd* (Plant, 2000; Gao et al., 2012), which could be related to mesoscale variability, especially given turbulence in the boundary layer (Benjamin et al., 1999).

In the initial test, we use 90° as the *dir* innovation threshold in BKG-QC. Note that any *dir* observation with innovation exceeding 90° is not regarded by the authors as necessarily indicating the observation is erroneous. Rather, the implementation is used to emphasise the impact of *dir* observations on the *spd* analysis in asm_uv in the situation that the vectors of background and observation are located in different quadrants. Although any *dir* innovation except zero could lead to this situation, it is assured to be rejected by restricting *dir* innovation to $<90°$.

Unless there is equivalency of the *dir* between observation and background, when assuming equal assimilation weights for wind observations in asm_uv and asm_sd, the scalar nature of *spd* generates a smaller *spd* innovation in asm_sd than the *spd* innovation converted from *u* and *v* innovations in asm_uv. Therefore, to avoid using *spd* observations with a bias towards larger *spd* innovations, the magnitude of the allowed *spd* innovation should be reduced in asm_sd, as compared to asm_uv.

Given that wind observations from different platforms with unique error characteristics (e.g. Plant, 2000; Drüe et al., 2008; Gao et al., 2012) are being used even when *dir* observation errors are rarely known, the varied nature of these input sources could increase the uncertainty of assimilation results.

This study is primarily designed to evaluate the performance of asm_sd in assimilating the satellite-derived AMV and surface-based dataset in Meteorological Assimilation Data Ingest System (MADIS),[6] which provides the best coverage over CONUS.

---

[6]madis.noaa.gov

When using an observation that is already assimilated into the background for verification reference, the obtained analysis correlates with the observation; thus, the verification for experiments may be biased because aliasing will inherently favour the experiment with larger assimilation weights for observations. This study evaluates model analyses and short-range forecasts against RAOB, which were not used in the assimilation, and are thus fully independent from analyses and forecasts. Finally, a precipitation event that occurred during the experimental period was chosen to further explore the indirect impacts of asm_sd on precipitation prediction in the full-cycle assimilation scheme. The precipitation reference is National Centers for Environmental Prediction (NCEP) Stage IV analysis with a resolution of 4 km (Lin and Mitchell, 2005).

The remainder of the paper is arranged as follows. In Section 2, we provide an overview of the new method and discuss distinctions concerning BKG-QC between asm_uv and asm_sd by using two cases. Section 3 describes the model configuration, the estimation of observation errors of *spd* and *dir*, and experiment design. The statistical results of evaluation and a precipitation case study are presented in Section 4. Finally, conclusions and an outlook for future research are provided in Section 5.

2. BKG-QC in the assimilation of wind speed and direction

The formulation of asm_sd apart from the details of BKG-QC is described in Huang et al. (2013). In brief, the variables related to wind in the innovation vector, observation error covariance and observation operators that participate in the cost function [Huang et al., 2013; eq. (1)] are transformed from u and v in asm_uv to *spd* and *dir* in asm_sd. Thus, the observation error covariance matrix $\mathbf{R}_{\mathrm{asm\_sd}}$ in asm_sd has variances of observation errors of *spd* and *dir* on the diagonal, replacing u and v in $\mathbf{R}_{\mathrm{asm\_uv}}$:

$$\mathbf{R}_{\mathrm{asm\_uv}} = \begin{pmatrix} \ddots & 0 & 0 & 0 \\ 0 & \sigma_u^2 & 0 & 0 \\ 0 & 0 & \sigma_v^2 & 0 \\ 0 & 0 & 0 & \ddots \end{pmatrix} \Rightarrow \mathbf{R}_{\mathrm{asm\_sd}}$$

$$= \begin{pmatrix} \ddots & 0 & 0 & 0 \\ 0 & \sigma_{spd}^2 & 0 & 0 \\ 0 & 0 & \sigma_{dir}^2 & 0 \\ 0 & 0 & 0 & \ddots \end{pmatrix} \quad (1)$$

In this study, the observation errors of u and v in asm_uv, σ_u and σ_v, employ the default errors defined in the WRFDA error table (Kalnay et al., 1996), and the observation errors of *spd* and *dir*, σ_{spd} and σ_{dir}, will be estimated in the next section.

The basic procedures of quality control, which are performed on observations before assimilation, include assessing vertical consistency (super adiabatic and wind shear checks) and a dry convective adjustment. Additionally, like in most data assimilation systems, the innovation and observation error are used in BKG-QC in WRFDA to determine data retention. Any observation y_i is rejected if

$$d_i > n \times \sigma_i \quad (2)$$

where d_i is the innovation (i.e. observation y_i minus the corresponding background), σ_i is the error for observation y_i, and n represents a fixed multiple of the observation error, which is set to 5 as default in WRFDA.

As stated above, asm_sd can generate a smaller *spd* innovation than asm_uv due to the scalar nature of *spd* under certain conditions. This conclusion can be explained similarly by Huang et al. (2013; Fig. 8), where u and v differences from reference are roughly 1.6 times of *spd* difference. Based on the statistics, n is defined as 3 for *spd* BKG-QC in asm_sd for this study.

In asm_sd, y_i and σ_i denote the *spd* or *dir* observation and its observational error, respectively. Thus, a *spd* or *dir* observation can be retained or directly screened out. However, eq. (2) is not able to effectively block a *spd* or *dir* observation grossly in error from being assimilated in asm_uv, because u and v innovations are not necessary for assessing eq. (2) when *spd* and *dir* innovations meet the requirements. Two cases illustrated in Fig. 1 present the differences in BKG-QC between asm_uv and asm_sd, where the *spd* observations and backgrounds are assumed to be equal for simplification, and *spd* observation error is defined as $2 \, \mathrm{ms}^{-1}$.

In case 1 (OBS1 and blue BKG1), a *dir* component of OBS1 with innovation exceeding 90° is rejected and only the *spd* component is assimilated into the analysis in asm_sd. By comparison, the u component of OBS1 is contaminated by the *dir* component being grossly in error, and even with an innovation score of $9.0 \, \mathrm{ms}^{-1}$ (less than 5x the observation error, $10.0 \, \mathrm{ms}^{-1}$) it is still assimilated into asm_uv. The assimilation produces a *spd* analysis falling outside the interval defined by the background and observation, as in Huang et al. (2013; Fig. 1).

In extreme situations, when assuming the equality of observation error and background error, the OBS1 and green BKG1 (with magnitudes $\sim 4.7 \, \mathrm{ms}^{-1}$) will produce zero *spd* analysis in asm_uv. It would be preferable for a reasonable *spd* analysis to maintain a magnitude close to both the background and observation ($\sim 4.7 \, \mathrm{ms}^{-1}$). Based on this case, there will always be a set of u and v observation errors leading to a *spd* analysis of zero in asm_uv when the *dir* innovation exceeds 90°, regardless of the magnitude of *spd* in background and observation.

In case 2, OBS2 is a good observation to be used in asm_sd; however, the *u* component of OBS2 is rejected in asm_uv due to the *u* innovation being larger than $10\,ms^{-1}$. Thus, the positive impacts of the good observation are lost in asm_uv. Although these counterexamples cannot lead to a conclusion that BKG-QC in asm_sd is uniformly superior to that of asm_uv, the former is more effective and reasonable than the latter based on these two simple cases. Typically, situations like case 1 are often observed near the surface, and situations similar to case 2 more frequently occur at higher altitudes.

3. Experimental framework

3.1. Model configuration

The Weather Research and Forecasting (WRF) model (Skamarock et al., 2008) was run with 15-km grid spacing on a 334×223 horizontal grid domain covering the CONUS and surrounding oceans (Fig. 2), using 37 vertical levels laid out with the model top at $50\,hPa$. The MADIS AMV and surface (including temperature, relative humidity and surface pressure in addition to *spd* and *dir*) datasets are used in this study. The experimental domain is shown in Fig. 2, as an example of the observation distributions on 0000 UTC 1 August 2013. Compared with the average distribution of AMV by time window, most surface data are centred ± 1 h around the analysis time, which improves the accuracy of assimilation by narrowing the time gap between the background and observations.

The experimental window begins at 0000 UTC 1 August 2013 and lasts for 2 weeks. The assimilation employs 3D-Var, and runs four times at 0000, 0600, 1200 and 1800 UTC per day with 6-h cycling (i.e. the 6-h forecast initialised from the previous analysis is considered as background). The time window of the assimilation was 3 h on either side of the analysis time. The National Meteorological Center (NMC) method (Parrish and Derber, 1992) was employed to generate the regional background error covariance using the prior 1-month of differences between WRF 12 and 24-h daily forecasts, replacing the existing global estimation (Wu et al., 2002). Lateral boundary conditions for WRF forecasts were provided by NCEP $0.5° \times 0.5°$ global forecasts.

3.2. The wind speed and direction observation errors

The estimation of *spd* and *dir* observation errors is implemented by first calculating the background error generated by the NMC method for the variables *u*, *v*, *spd* and *dir* and scaling the observation errors of *u* and *v* from the existing WRFDA system:

$$\sigma^o_{spd/dir} = \sigma^b_{spd/dir} \times \frac{\sigma^o_{u/v}}{\sigma^b_{u/v}} \qquad (3)$$

Here, the subscripts (*u*, *v*, *spd* and *dir*) denote the assimilation variables in asm_uv and asm_sd; σ^o and σ^b are the standard deviations of observation error and background error, respectively; $\sigma^o_{u/v}$ is defined based on WRFDA, and
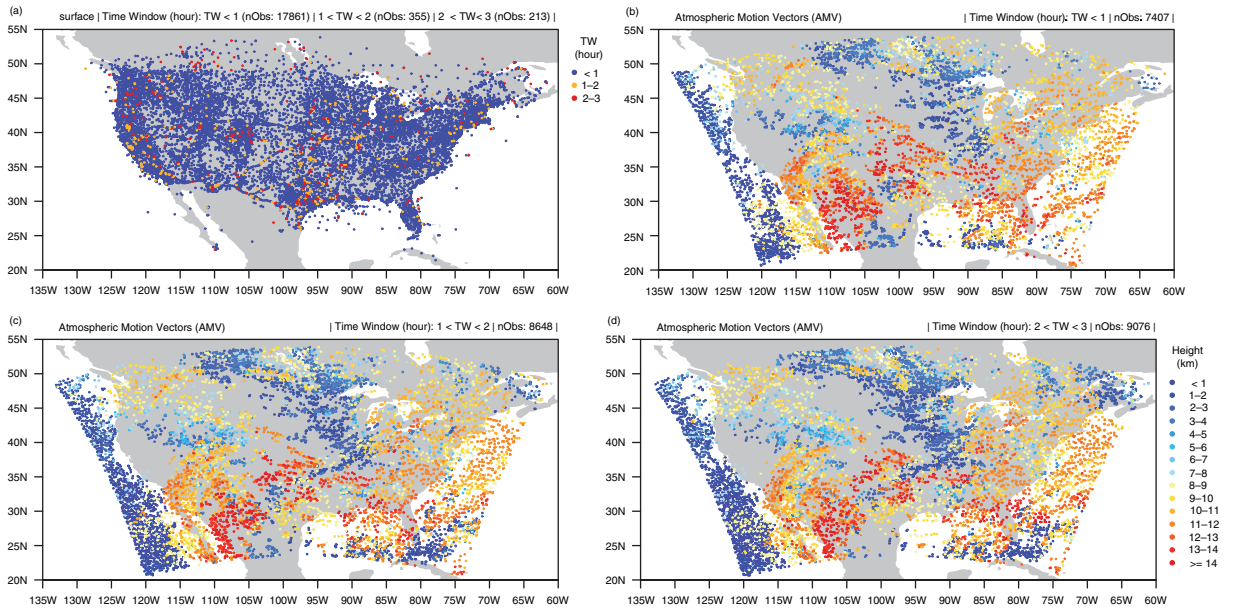

Fig. 2. The experimental domain and the spatial and temporal distributions of MADIS surface (a) and satellite-derived Atmospheric Motion Vectors (AMV) observations (b–d) at 0000 UTC 1 August 2013 with the time window of ± 3 h. The observation count (nObs) is shown by time window on top. The time window is denoted by colours in (a), and the vertical height is denoted by colours in (b–d).

(a) wind speed background error estimated

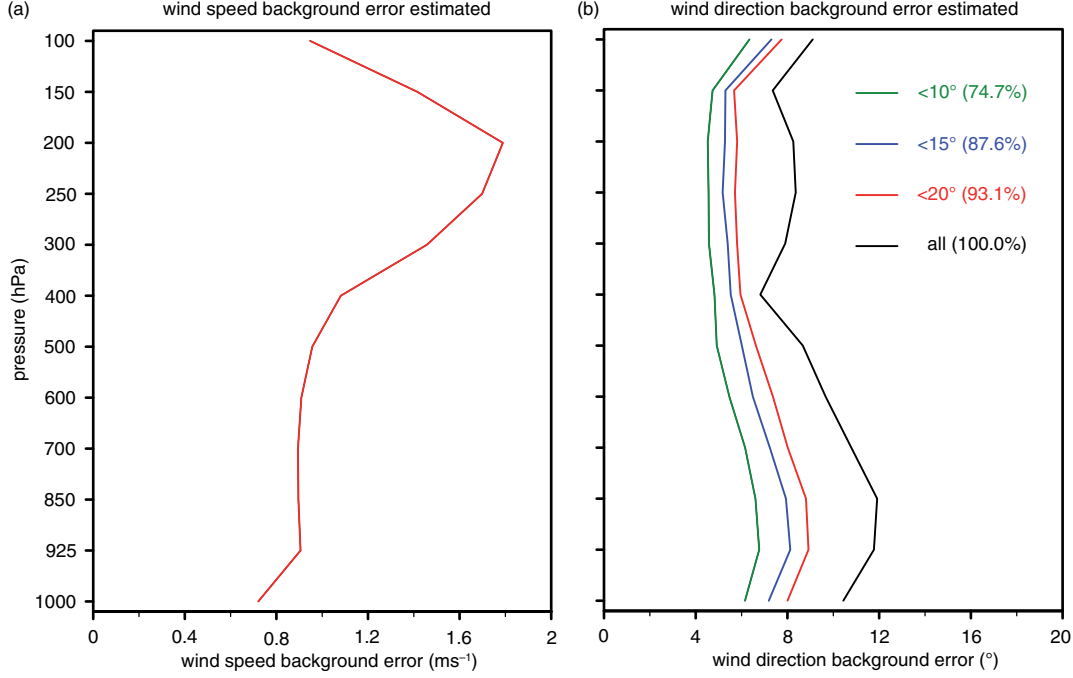(b) wind direction background error estimated

Fig. 3.   The background errors calculated by the National Meteorological Center (NMC) method for wind speed (a) and direction (b). The background errors are estimated by eq. (5). The degree number in (b) denotes the maximum background error of wind direction allowed for the statistics, and the percent number denotes how many grid points survive the statistics.

$\sigma^b_{spd/dir}$ and $\sigma^b_{u/v}$ will be estimated by eqs. (4) and (5). Equation (3) ideally results in similar assimilation weights for wind observations between asm_uv and asm_sd.

For any observation y_i, the analysis increment $(x_a - x_b)$ is proportional to the background error covariance $\mathbf{B}_i$ assuming a single model variable x_i:

$$x_a - x_b = \mathbf{B}_i(\sigma^2_b + \sigma^2_o)^{-1}(y_i - x_i) \qquad (4)$$

[also see eq. (8) in Huang et al., 2009]. Derived from eq. (4), we have:

$$\sigma_b = \sigma_o \times \left(\frac{(x_b - x_a)}{(x_a - y_i)} \right)^{\frac{1}{2}} \qquad (5)$$

By using eqs. (4) and (5), the background errors of u, v, spd and dir, i.e. σ^b_u, σ^b_v, σ^b_{spd} and σ^b_{dir}, were calculated, respectively, by single observation tests (SOT) on every six grid points on 12 standard pressure levels over the entire experimental domain. The SOT assimilates single u, v, spd or dir components per time at a chosen horizontal grid point and vertical level.

Therefore, the SOT can provide the background error for u, v, spd or dir at the observation location, which does not include the impact of the horizontal correlation from any other observation. The estimated background errors of spd and dir by pressure are shown in Fig. 3. Because spd background errors are similar to the background errors of
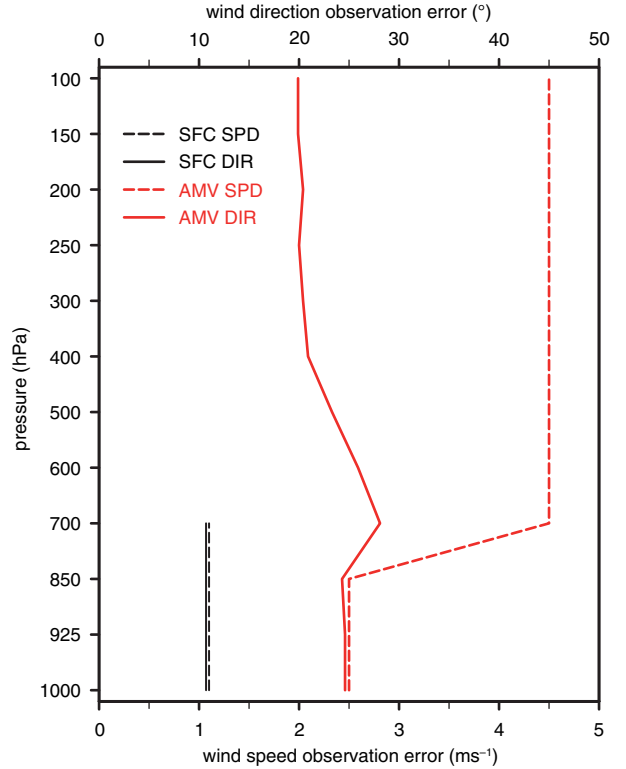

Fig. 4.   The observation errors of wind speed (SPD) and direction (DIR) estimated by eq. (3) for MADIS surface wind (SFC) and satellite-derived Atmospheric Motion Vectors (AMV) observations.
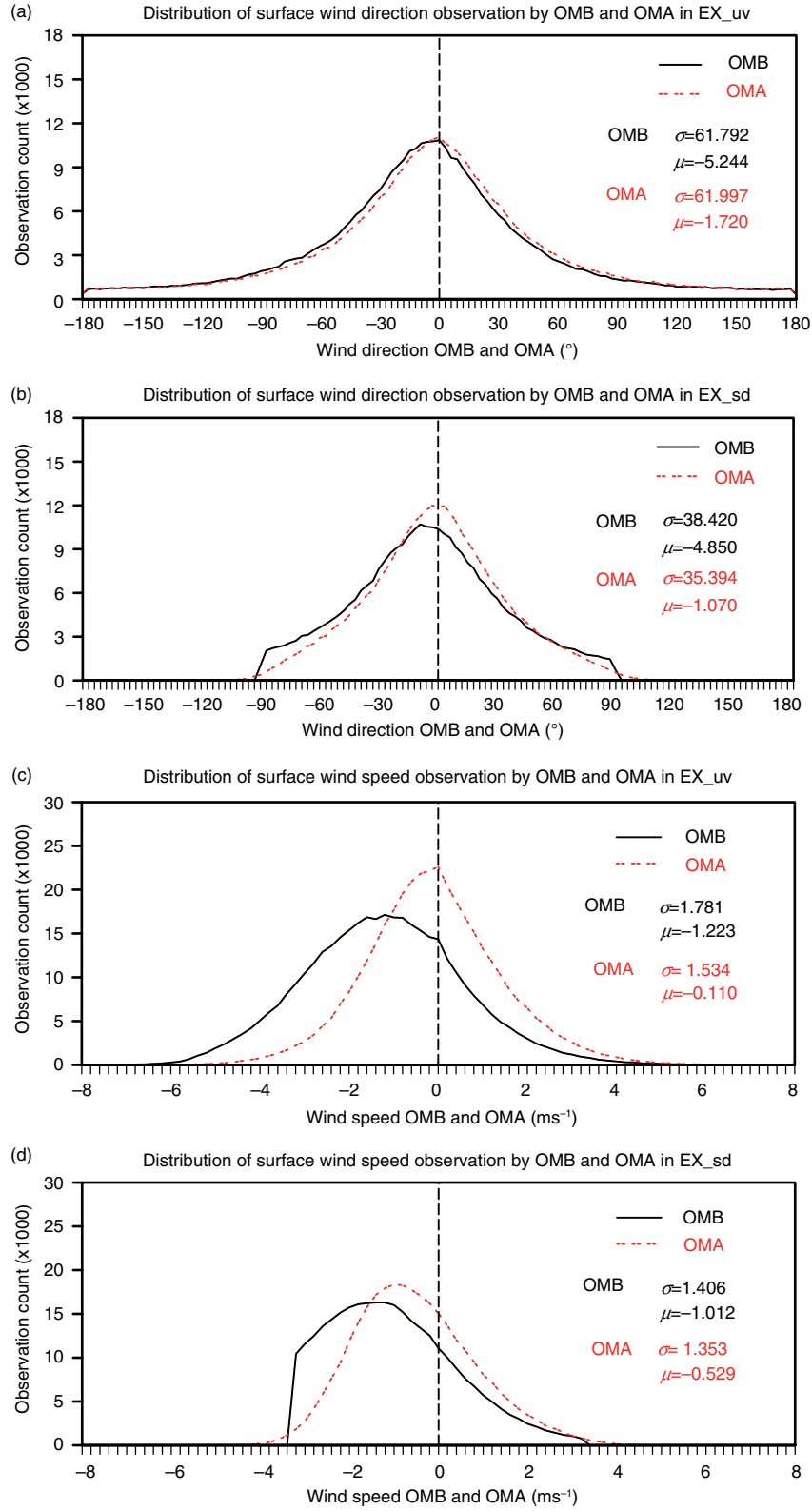
Fig. 5. The distribution of surface wind direction (a–b) and speed (c–d) observations by observation minus background (OMB, black lines) and observation minus analysis (OMA, red lines) in EX_uv and EX_sd. σ and μ in panels denote the standard deviation and bias of OMB and OMA, respectively.

u and *v* (not shown), the estimated *spd* observation error is close to the observation errors of *u* and *v*.

The default *spd* observation error in WRFDA is also used as the observation errors of *u* and *v* in asm_uv, and is employed as the *spd* observation error (σ_{spd}) for asm_sd in this study. The statistics of *dir* background error can be impacted from situations where grid points with background errors deviate greatly from the general range of the *dir* background error. To eliminate these unstable values, we set a series of maxima below which the *dir* background error on a grid point will be used in the calculation of the average *dir* background error. The resulting options for three similar profile patterns of *dir* background error are presented in Fig. 3b. By setting the maximum to 20°, *dir* background errors decrease notably at every pressure level, yet 93% of grid points are still used in the statistics. Therefore, *dir* observation errors are estimated by using the vertical profile of *dir* background errors with a maximum of 20° (red line).

In Fig. 3, the background errors of *spd* and *dir* vary with height, an effect also discussed for observation errors in Gao et al. (2012). Generally, *spd* (background and observation) error increases with height, and the opposite is true for *dir*. However, this pattern is not uniformly true, as shown by the profile of *dir* observational errors indicated in Fig. 4. Note that the *spd* and *dir* observation errors estimated here are not intended to maintain consistency with sensor errors, or to agree with the statistics in WRFDA, but to get similar assimilation weights in asm_uv and asm_sd between *u* and *v* errors and *spd* and *dir* errors. For surface observations, constant *spd* and *dir* observation errors are used despite the fact that instrumentation may be placed at slightly different heights.

3.3. The experiment design

The differences of analyses produced by asm_uv and asm_sd result from the impacts of differences in BKG-QC and the assimilation method itself. To evaluate the performance of asm_sd in these aspects, four assimilation experiments are designed as follows:

(1) EX_uv is considered the control run, conventionally employing asm_uv by using the default observation errors defined in WRFDA;
(2) EX_sd employs asm_sd by using the estimated observation errors of *spd* and *dir* in Fig. 4;
(3) EX_sd_uvobs employs asm_sd as EX_sd, but assimilates the same observations used in EX_uv per cycle;
(4) EX_sd_sfc employs asm_sd and asm_uv for assimilating surface wind and AMV, respectively.

Since any other observation variable except wind employs the same assimilation scheme among these four experiments, we assume that the differences of wind analyses between EX_uv and EX_sd are derived from the new assimilation method, although it partly includes the impact from the different background at every cycle assimilation. By comparing EX_uv with EX_sd_uvobs, the contribution of the assimilation method itself can be verified due to the same observations used. Thereafter, the impact of BKG-QC can be estimated linearly by subtracting the improvements produced by EX_sd_uvobs from those produced by EX_sd, over EX_uv. Likewise, the exclusive impact of asm_sd on the assimilation of surface wind or AMV observations can be tested by comparing EX_uv with EX_sd_sfc or EX_sd with EX_sd_sfc, respectively.

4. Results

4.1. Distribution of observation by residuals of observation from background and analysis

The usage and weight of the observations in the analysis can be demonstrated by the statistical residuals of observation minus background (OMB) and observation minus analysis (OMA). The distributions of surface *dir* and *spd* observations by the residuals of OMB and OMA in EX_uv and EX_sd are presented in Fig. 5. From Fig. 5a, a large number of *dir* observations with innovations (i.e. OMB) exceeding 90°, about 15.0% of all surface *dir* observations, are assimilated in EX_uv. It appears that BKG-QC in asm_uv does not have a particularly stringent impact on the retention of *dir* observations.

By comparison, *dir* observations with innovations larger than 90° are screened out directly by BKG-QC in EX_sd (Fig. 5b), which significantly reduces the standard deviation (σ) and bias (μ) of OMB and OMA. It is also worth mentioning that for *dir*, OMA is even larger than OMB in EX_uv (Fig. 5a), denoting that cost function minimisation in asm_uv does not necessarily converge for *dir*.

With respect to *spd*, OMB is biased with the minimum value of $-7.1\,\text{ms}^{-1}$ and maximum of $5.4\,\text{ms}^{-1}$ in EX_uv (Fig. 5c). Compared with a sharp cutoff of OMB at $-3.3\,\text{ms}^{-1}$ in EX_sd (Fig. 5d), where the BKG-QC directly screens out *spd* observations meeting eq. (2), BKG-QC of *u* and *v* in EX_uv are not able to effectively reject *spd* observations with large *spd* OMB, representing a source of strong bias.

As discussed earlier, when *dir* observations with innovation exceeding 90° are assimilated in asm_uv, *spd* analysis may be reduced because of the vector nature of *u* and *v*. The negative bias in surface *spd* OMB means that the magnitudes of most *spd* observations are smaller than the background. Therefore, the *spd* analysis produced by asm_uv is a
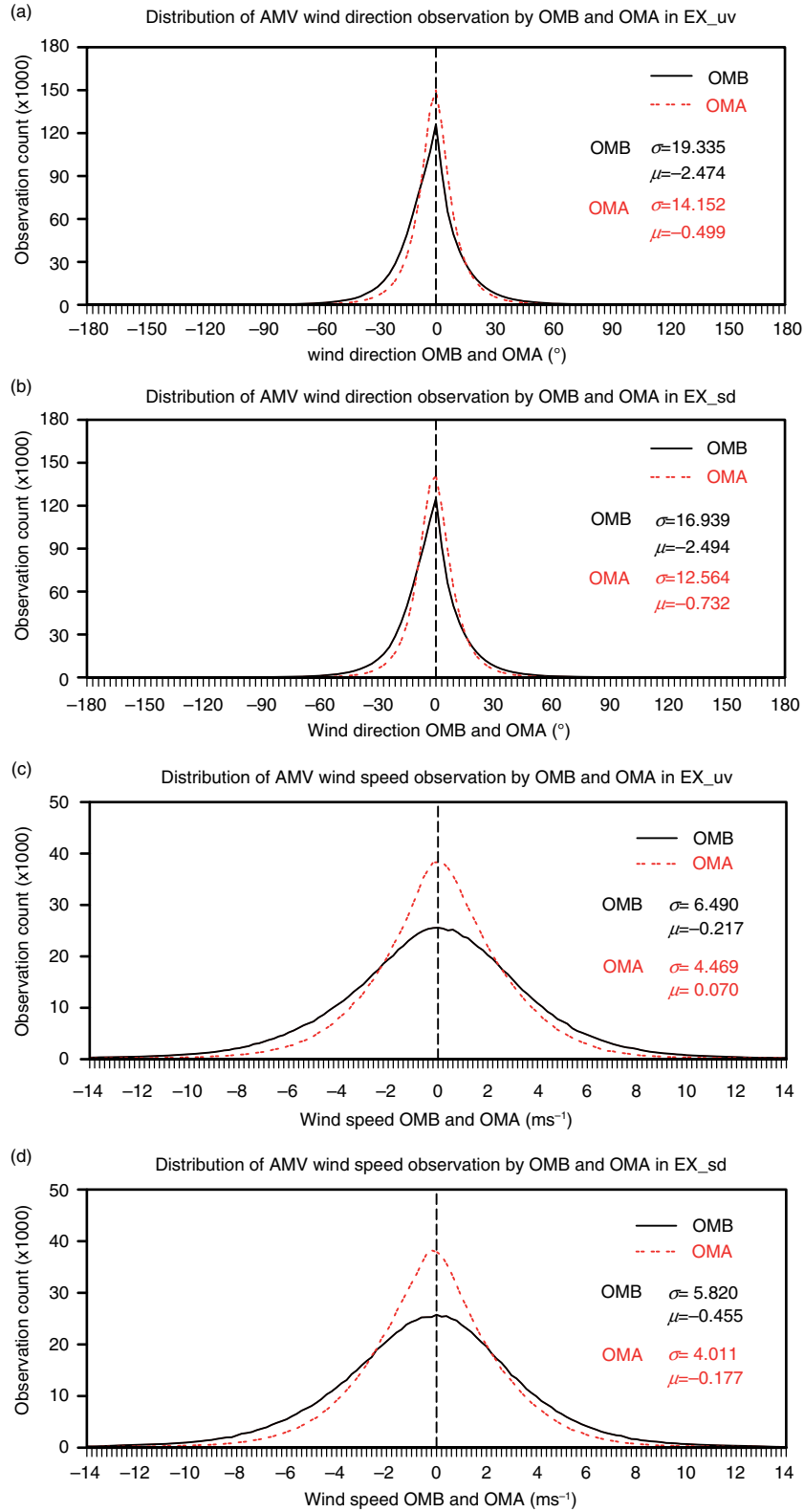
Fig. 6. The distributions of satellite-derived Atmospheric Motion Vectors (AMV) wind direction (a–b) and speed (c–d) observations by observation minus background (OMB, black lines) and observation minus analysis (OMA, red lines) in EX_uv and EX_sd. σ and μ in panels denote the standard deviation and bias of OMB and OMA, respectively.
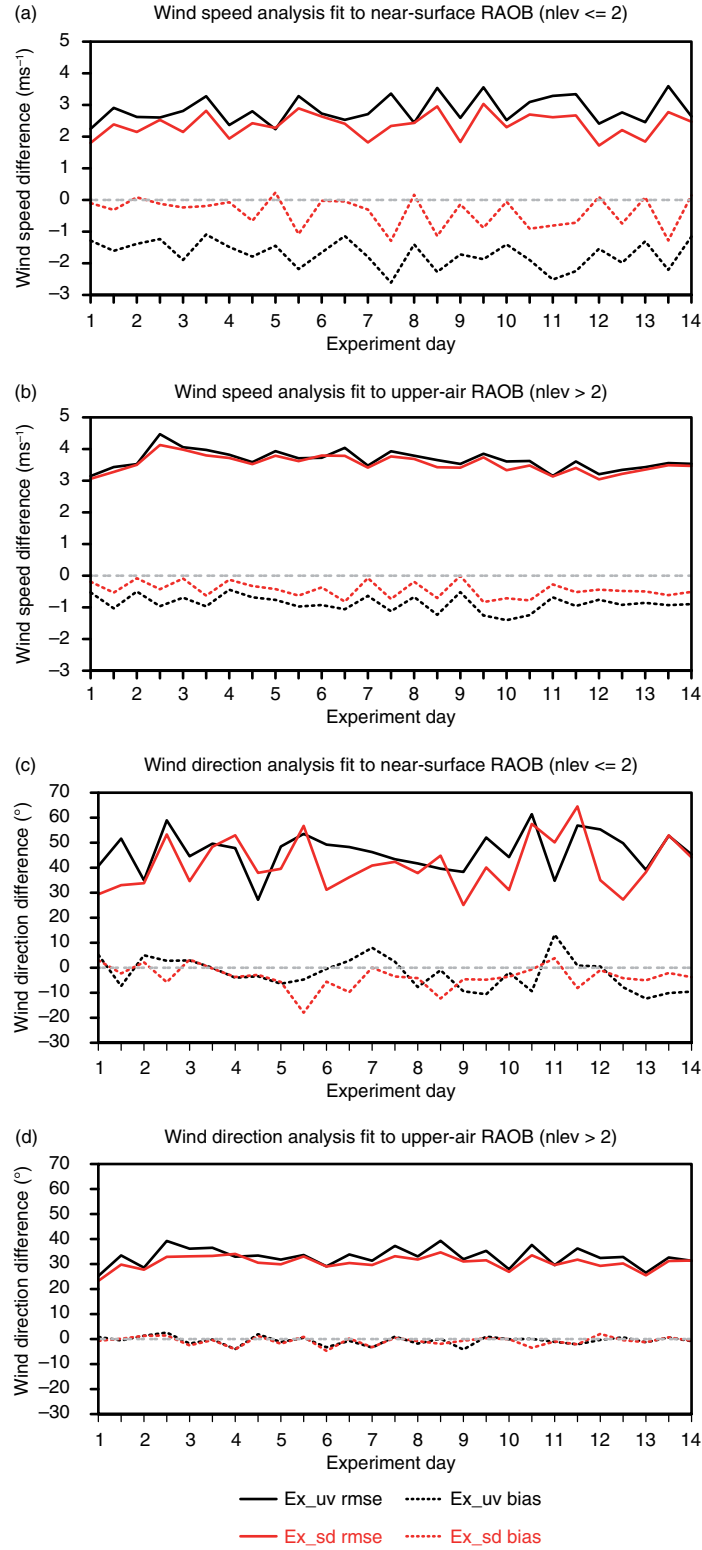
Fig. 7.   The time series of rmse and bias of wind speed (a–b) and direction (c–d) analyses in EX_uv and EX_sd fit to rawinsonde observations (RAOB). Near-surface RAOB (nlev ≤ 2) denotes RAOB available on two lowest height levels; upper-air RAOB (nlev > 2) denotes RAOB available above two lowest height levels. Black and red lines are statistics in EX_uv and EX_sd; solid and dot lines represent rmse and bias, respectively.
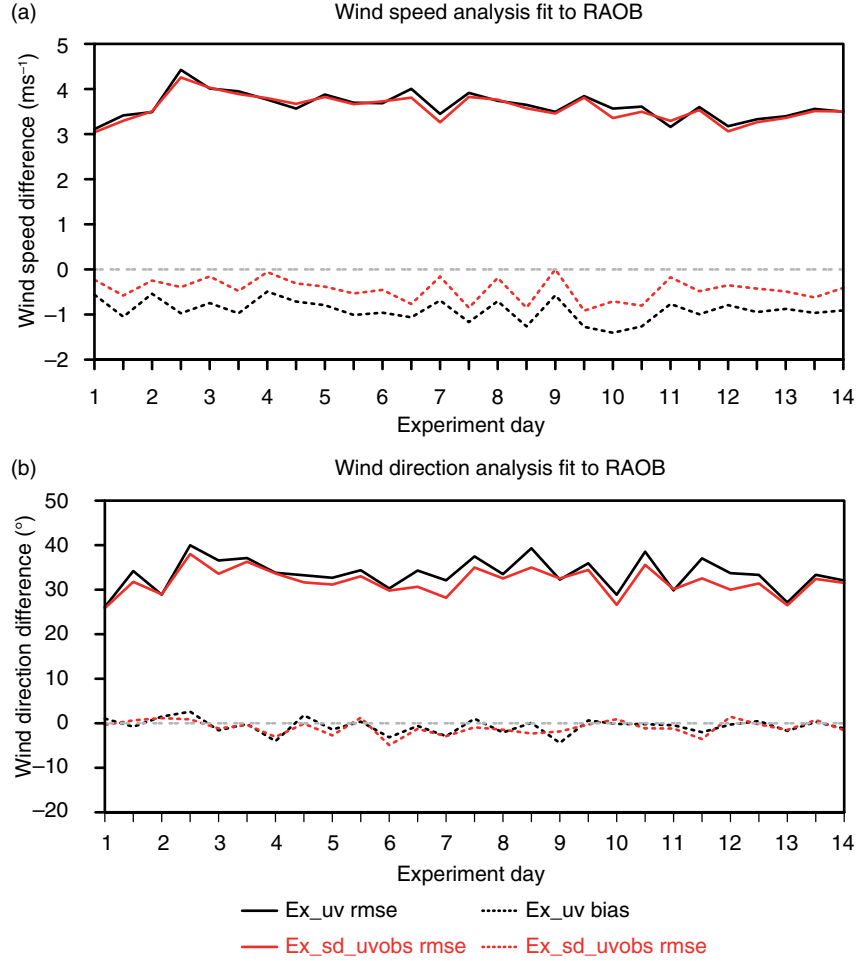
Fig. 8. The time series of rmse and bias of wind speed (a) and direction (b) analyses in EX_uv and EX_sd_uvobs fit to rawinsonde observations (RAOB). Black and red lines are the statistics in EX_uv and EX_sd_uvobs; solid and dot lines represent rmse and bias, respectively.

closer fit to surface *spd* observations than the *spd* analysis produced by asm_sd. As a result, a Gaussian-like pattern of OMA with a relatively small bias ($-0.11\,\mathrm{ms}^{-1}$) is seen in EX_uv (Fig. 5c).

By comparison, the bias of surface *spd* OMA in EX_sd is located between the bias of surface *spd* OMB and zero (Fig. 5d), demonstrating that the surface *spd* analysis is reasonably distributed between the observations and background. Due to the fact that surface *spd* observations are biased in this study, it is acceptable to assume that the *spd* analysis will over-fit the observations if a near-zero bias exists in OMA. In reality, the uncorrected bias in surface *spd* observations can be used to prove that the assimilation of biased *spd* observations is not the primary reason for the large bias of the *spd* analysis in EX_uv.

The distribution of AMV *dir* and *spd* observations by the residuals of OMB and OMA in EX_uv and EX_sd are shown in Fig. 6. The AMV observations reveal a good fit to

the background, such that the BKG-QC in EX_uv and EX_sd only account for a 0.37% difference in observation counts. Although AMV *dir* OMB mainly appear inside the bounds of $\pm 60°$ (Fig. 6a and b), the *dir* observations located in different quadrants from the background still represent approximately 8.0% of all *dir* observations in EX_uv, and these can be expected to generate some significant impacts on *spd* analysis in EX_uv.

4.2. Verification of analysis

The statistical verification presented below is the difference of the analyses and forecasts from RAOB in the form of root-mean-square (rms) and average (bias). Considering the launch time of rawinsondes, the verification is only performed at 0000 and 1200 UTC each day.

The rms difference/error (hereafter referred to as rmse) and bias of *spd* and *dir* analyses fit to RAOB in EX_uv and
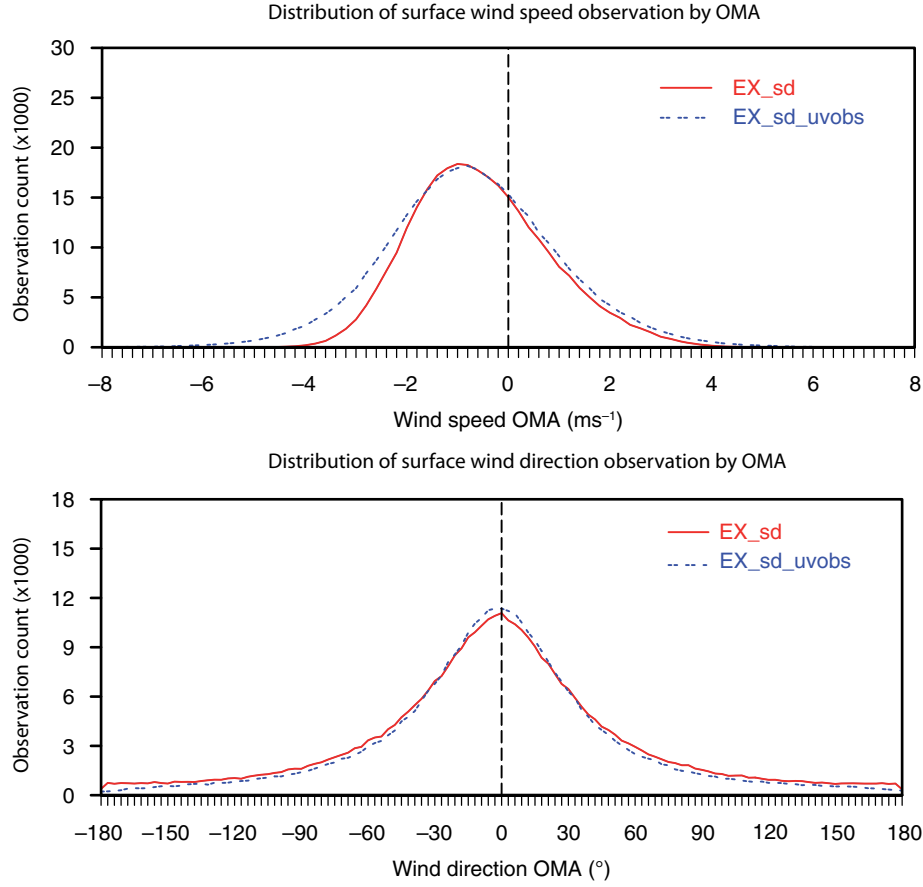
Distribution of surface wind speed observation by OMA

Distribution of surface wind direction observation by OMA

Fig. 9. The distribution of surface wind speed observations by observation minus analysis (OMA) in EX_sd and EX_sd_uvobs (a) and of surface wind direction observations by observation minus analysis (OMA) in EX_uv and EX_sd_uvobs (b).

EX_sd is presented in Fig. 7. In Fig. 7a and c, the RAOB data available on the two lowest height levels are used as a reference to present the verification of near-surface wind analysis, where the statistical differences between EX_uv and EX_sd are assumed to be derived from the impact of asm_sd on surface wind data assimilation. Likewise, in Fig. 7b and d, the RAOB data available above the two lowest height levels are used as a reference for verification of upper-air wind analysis, where the statistical differences between EX_uv and EX_sd are assumed to originate from the impact of asm_sd on AMV data assimilation.

Based on rmse, both *spd* and *dir* analyses from EX_sd come closer to RAOB than EX_uv, and the improvement from EX_sd is notable for upper-air locations (Fig. 7b and d) on 1200 UTC 2 August, when the associated precipitation event is examined in Section 4.4. Additionally, the biases of the *spd* analyses in EX_sd dramatically decrease by 77.5% and 53.0% for near-surface and upper-air locations, respectively (Fig. 7a and b).

Compared with EX_sd, the bias of the *spd* analysis in EX_uv presents as an inherent discrepancy (cf. Fig. 7a and b),

and is likely related to the assimilation method of *u* and *v*. As stated above, the BKG-QC only makes a difference of 0.37% in AMV observation counts between EX_uv and EX_sd; therefore, the bias of the *spd* analysis for upper-air (Fig. 7b) is mainly a function of the assimilation methodology of *u* and *v*. In other words, the larger improvements in bias from EX_sd for the near-surface *spd* analysis also include the impacts of BKG-QC. The BKG-QC results in surface *dir* observations with innovations exceeding 90°, which account for 15% of all surface *dir* observation assimilated in EX_uv, but are rejected in EX_sd (cf. Fig. 6a with b). These *dir* observations also produce an inherent impact on the *spd* analysis in addition to *spd* observations in asm_uv.

4.3. Impacts of BKG-QC and assimilation methods on analysis

The improvements from asm_sd are produced jointly from the new method and BKG-QC. The time series of rmse and bias of *spd* and *dir* analyses in EX_uv and EX_sd_uvobs is presented in Fig. 8.

The BKG-QC difference between asm_uv and asm_sd may be ignored in the two experiments due to fact that the same observations have been assimilated. Thus, the new assimilation method is assumed to produce the analysis differences between EX_uv and EX_sd_uvobs. As a result, the impact of BKG-QC can be estimated linearly by subtracting improvements produced by EX_sd_uvobs from the improvements produced by EX_sd compared to EX_uv. The improvements of *dir* analysis, shown by the rmse decreasing from 6.9% in EX_sd to 5.0% in EX_sd_uvobs, suggest that the new assimilation method produces a more positive impact on the *dir* analyses than BKG-QC, which only contributes 1.9%.

In terms of *spd*, BKG-QC in asm_sd plays an important role in improving the rmse of *spd* analyses by effectively screening out biased *spd* observations (Fig. 5d). However, the *spd* bias is largely unchanged with improvements of 54.8% in EX_sd and 54.4% in EX_sd_uvobs. This result demonstrates that the improvement on *spd* bias is mainly derived from the new assimilation method, i.e. the independent impact of *spd* (*dir*) observations on the *spd* (*dir*) analysis. This conclusion is also supported by Fig. 9, which shows the *spd* OMA for EX_sd and EX_sd_uvobs, as well as the *dir* OMA for EX_uv and EX_sd_uvobs.

Compared with EX_uv, the cost function related to *dir* converges in EX_sd_uvobs; therefore, the standard deviation of *dir* OMA in EX_sd_uvobs is smaller than that in EX_uv (Fig. 9b). However, as seen in Fig. 9a, unlike in EX_uv (Fig. 5c), the assimilation of *dir* observations with large innovations (e.g. $>90°$) in EX_sd_uvobs does not prompt *spd* analyses to over-fit to *spd* observations. The main differences of *spd* OMA between EX_sd_uvobs and EX_sd have ranges of $-6\,\mathrm{ms}^{-1}$ and $-2\,\mathrm{ms}^{-1}$, and these are actually derived from the assimilation of more *spd* observations with large negative OMB, which are rejected in EX_sd but used in EX_uv (Fig. 5c and d).

As stated above, the improvement on the bias of *spd* analyses is the primary feature of asm_sd. As such, a qualitatively consistent conclusion should also exist when employing asm_sd for the assimilation of either surface wind or AMV observations. The bias profile of *spd* analyses in EX_uv, EX_sd, and EX_sd_sfc is shown in Fig. 10. Below 700 hPa, the significant positive impact produced by asm_sd on surface *spd* data assimilation can be seen by comparing EX_uv and EX_sd_sfc. Compared to upper-air locations, more improvements are generated on surface *spd* analyses because BKG-QC in asm_sd plays a more important role in screening out surface *dir* observations with large *dir* innovations than AMV *dir* observations. In terms of AMV, although there is a good fit to the background (Fig. 6a), the *dir* observations that have different quadrants from the background still generate a notable impact on the bias of the *spd* analysis. This result strongly supports
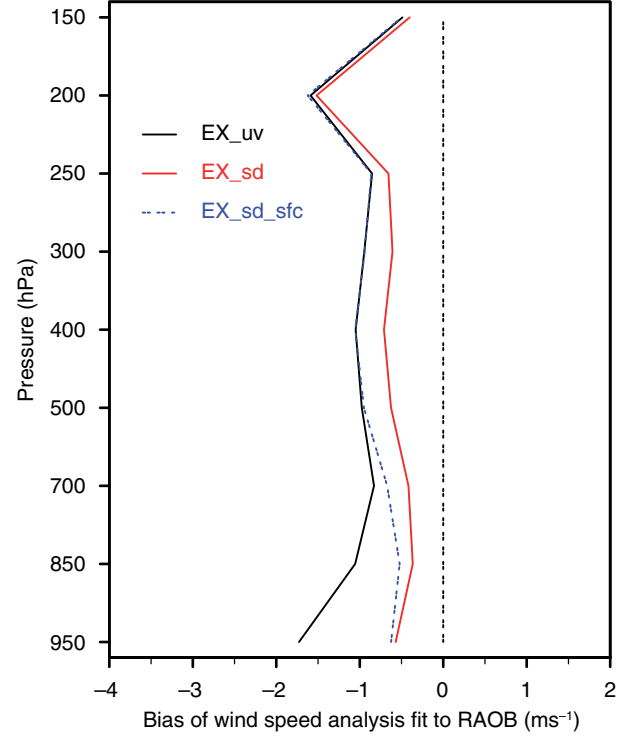

Fig. 10. The biases of wind speed analyses in EX_uv, EX_sd and EX_sd_sfc fit to rawinsonde observations (RAOB).

the importance of the independent impact of the wind observation variables on the wind analysis.

4.4. Verification of forecast

4.4.1. The statistical characteristics. The rmse and bias of *spd* and *dir* forecasts of all cycles by forecast lead time are presented in Fig. 11. The forecast improvements from asm_sd are mainly reflected in the bias of *spd* and rmse of *dir*, and are consistent with the conclusions for the analyses. Although the forecast differences decrease with lead time because the same lateral boundary conditions are employed for the comparative experiments, the bias of spd forecast in EX_sd are still present at 48 h.

From the vertical profiles of 12-h forecast scoring (Fig. 12), *dir* forecast rmse in EX_sd is improved over EX_uv at all height levels, and the biases around 1000 hPa and 500 hPa in EX_sd are only little larger than EX_uv. The significant improvements on biases of the *spd* forecast in EX_sd can still be seen at all height levels; however, the near-surface improvements are reduced by the restriction of the lateral boundary condition (cf. Fig. 7a). The improvement in the rmse of *spd* forecasts in EX_sd are especially appreciable in light of the non-optimal configuration and tuning in EX_sd. Similar forecast scoring is seen for asm_sd without the negative impacts on *spd* forecasts, such as those near 400 hPa (Fig. 12a).

(a)

Wind speed forecast fit to RAOB

(b)

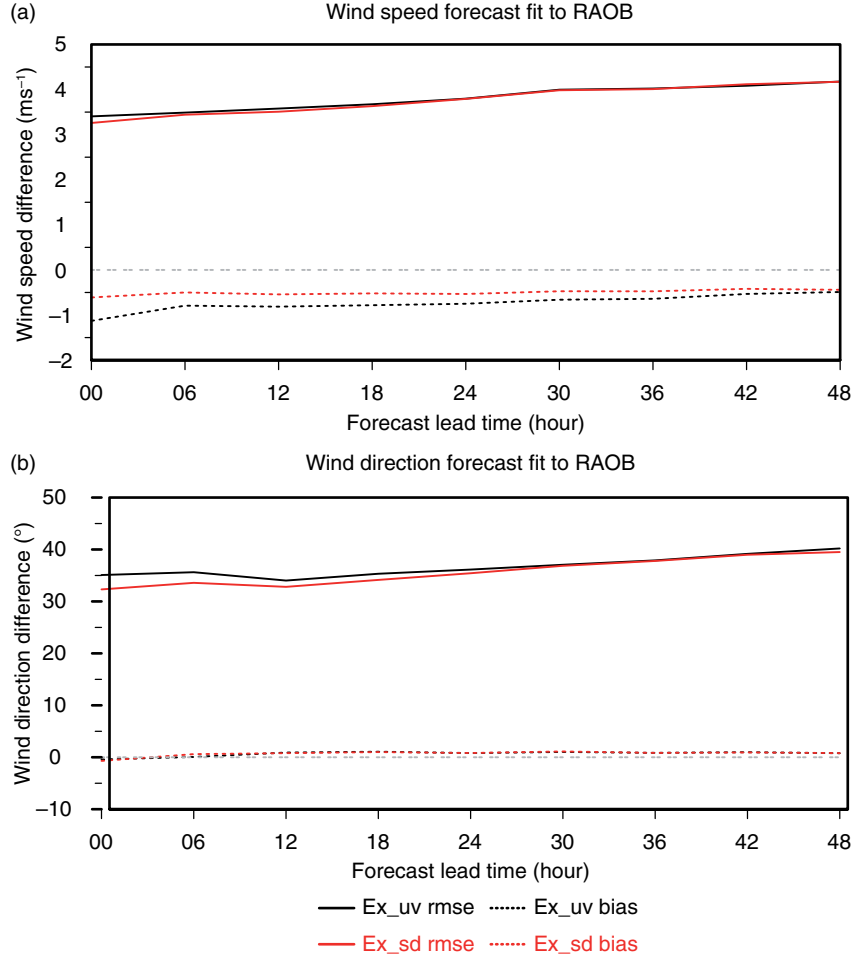Wind direction forecast fit to RAOB

Fig. 11.   The rmse and bias of wind speed and direction forecasts in EX_uv, EX_sd fit to rawinsonde observations (RAOB) by forecast lead time.

4.4.2. A case for illustration. In this section, we explore how the improved wind analysis and forecast affect precipitation prediction. In WRFDA, the background error covariance does not include the covariances between moisture and other state variables. Therefore, the different moisture analyses between asm_uv and asm_sd are derived from the cycling assimilation, where the wind forecast adjusts the distribution of moisture, and then the updated moisture forecast is accumulated into the subsequent timestep's background and analysis.

At 1200 UTC 2 August 2013, a stream of warm moist air flowed towards the Kansas/Missouri (KS/MO) border where a cold dry air mass was in place. A frontal shear line developed over northern Illinois (IL) and Indiana (IN) along the boundary between the two air masses. The 24-h accumulated precipitation was heaviest (116 mm) near KSGF station in Springfield, MO (black dot in Fig. 14a).

The vertical profiles of 12-h *spd* and *dir* forecasts valid at 1200 UTC 3 August 2013 fit to RAOB at KSGF station are shown in Fig. 13. Generally, the *spd* and *dir* predictions are improved in EX_sd mainly below 400 hPa. From Fig. 13a, both EX_uv and EX_sd under predicted *spd*. As a result, the warm moist air advection was reduced in the model. The negative difference between the *dir* forecast in EX_sd and RAOB below 700 hPa indicates that the predicted *dir* points to the north-northwest of the observed wind vector, which leads to a more westerly-tilting weather system with respect to observations. Compared to EX_sd, the *spd* and *dir* forecasts from EX_uv further exacerbate these problems.

A plot of precipitation, wind vectors, and specific humidity in the mixed layer is shown in Fig. 14. Three main differences in the prediction of precipitation location and intensity between EX_sd and EX_uv can be seen along the border of KS and MO, the northern portions of IL and IN, and in southern South Dakota (SD). As discussed for
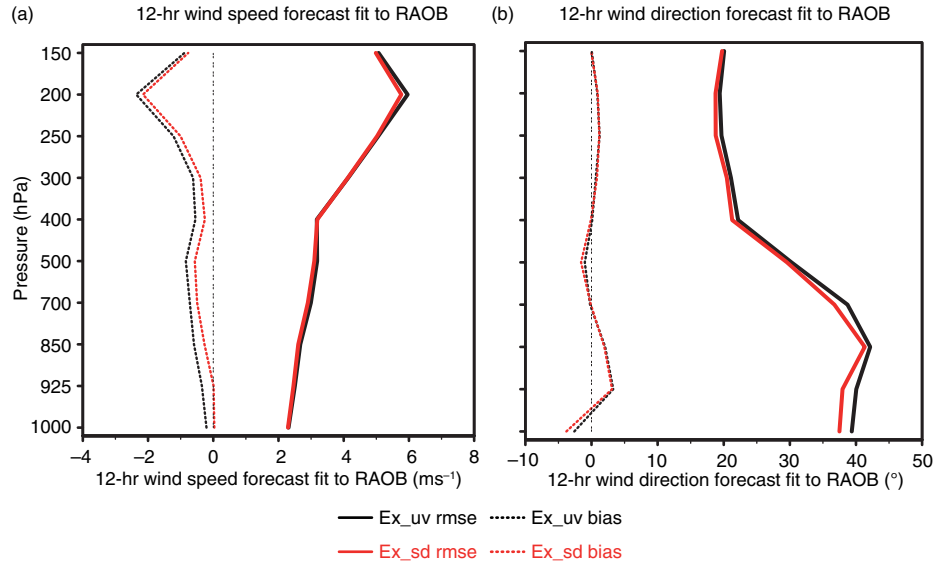
Fig. 12. The vertical profiles of rmse and bias of 12-h wind speed and direction forecasts in EX_uv and EX_sd fit to rawinsonde observations (RAOB).

Fig. 13, the weaker warm moist air advection in EX_sd reduces the precipitation intensity along the border of KS and MO in EX_sd. Meanwhile, the northwest-tilting *dir*, and the corresponding specific humidity gradient, lead to a prediction of the main precipitation area being located northwest of the observed precipitation maximum from the Stage IV analysis near KSGF (Fig. 14c). As expected,

the further westerly-tilting *dir* forecast in EX_uv fails to properly develop the primary precipitation zone in central KS (Fig. 14b).

Another key difference can be seen in southern SD, where weak winds exist in EX_sd (Fig. 14c). However, the stronger wind shear, coinciding with a moisture maxima, produces the main precipitation core over southern SD
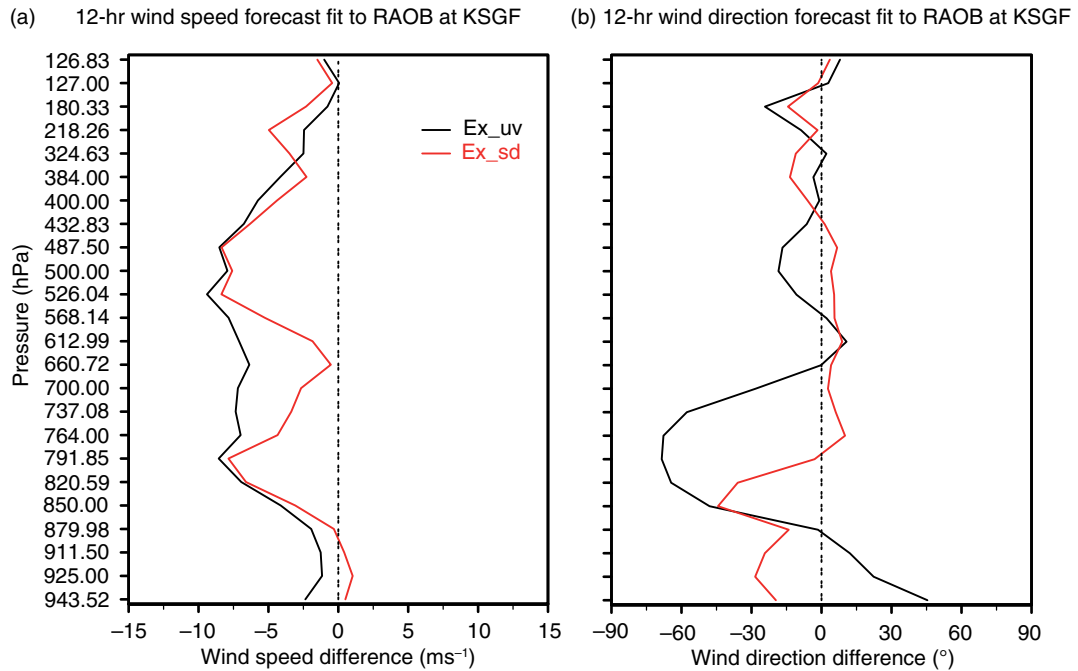

Fig. 13. The differences of 12-h wind speed and direction forecasts valid at 0000 UTC 3 August 2013 in EX_uv and EX_sd from rawinsonde observations (RAOB) at KSGF station in Springfield, Missouri.
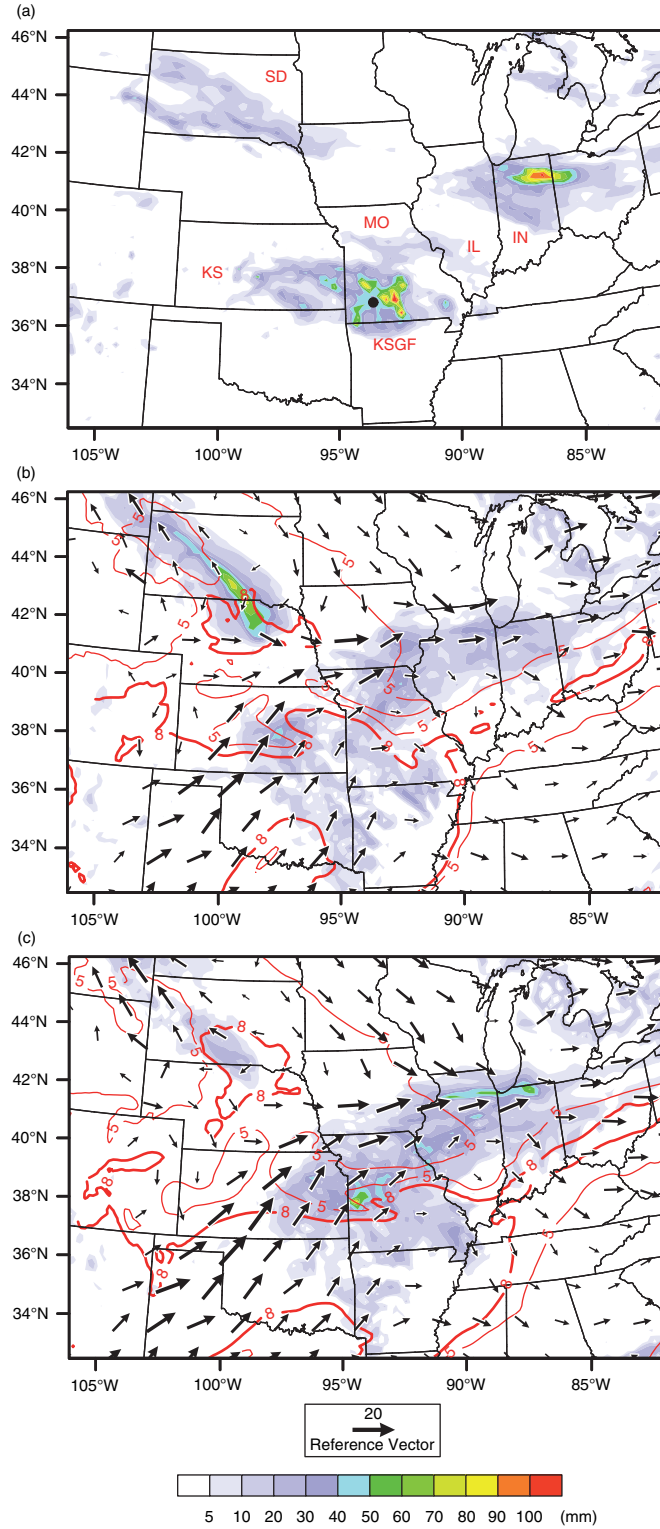
Fig. 14. The Stage IV 24-h accumulated precipitation analysis (shaded) valid at 1200 UTC 3 August 2013 in (a); the analyses of wind (vector) at 850 hPa and specific humidity (red line) at 700 hPa at 1200 UTC 2 August 2013 and 24-h accumulated precipitation forecasts (shaded) valid at 1200 UTC 3 August 2013 in EX_uv (b) and EX_sd (c). The unit for precipitation is mm, for specific humidity is g kg^{-1}, and for wind vector is ms^{-1}. The black dot in (a) denotes the rawinsonde station KSGF in Springfield, Missouri. South Dakota, Kansas, Missouri, Illinois and Indiana are abbreviated to SD, KS, MO, IL and IN, respectively.

in EX_uv (Fig. 14b). These results demonstrate that the improved wind forecast is able to improve the precipitation forecast by adjusting the wind-related factors driving the intensity and location of precipitation development via moisture advection.

5. Conclusion and outlook for further research

This paper presents a series of real-data experiments to evaluate the assimilation of wind observations in the forms of wind speed (*spd*) and direction (*dir*). The potential benefits of this method were verified over a continental United States domain for a 2-week period in the cycling assimilation. Satellite-derived Atmospheric Motion Vectors (AMV) and surface data from Meteorological Assimilation Data Ingest System (MADIS) were assimilated, and their *spd* and *dir* observation errors were estimated for the purpose of assigning similar assimilation weights for wind observations in asm_uv and asm_sd. Using rawinsonde observations (RAOB) and National Centers for Environmental Prediction (NCEP) Stage IV analysis as references, the statistical verification of the wind analyses, forecasts and a precipitation case study are presented.

Results demonstrate that the asm_sd produces better analyses and forecasts compared to asm_uv based on rmse and bias. Improvement up to 54.8% is generated by asm_sd for the bias of *spd* analyses, and persists through the 48-h forecasts despite using identical lateral boundary conditions. In a pilot test (EX_sd_uvobs) employing asm_sd, but assimilating the same observations as EX_uv, we show that the significant improvement in bias of *spd* analysis was primarily from the new assimilation method.

The background quality control (BKG-QC) in WRFDA is also a key factor in improvements of asm_sd over asm_uv. In the total rmse improvement of 3.7% for *spd* analyses and 6.9% for *dir* analyses, the 2.3% and 1.9% for *spd* and *dir* analyses are derived solely from the BKG-QC of asm_sd, respectively. Generally speaking, some benefits from asm_sd were produced from BKG-QC screening wind observations, but most benefits originated from the new assimilation method itself.

The indirect impacts of asm_sd on precipitation prediction were examined using an event which occurred during the experimental period. Results suggest that the asm_sd is able to improve the forecast of precipitation intensity and location by improving the prediction of wind-related dynamics.

Given the limitations of the experimental design, some differences may exist with operational applications. The observational errors are not optimally tuned when it comes to the assimilation weights between observations and background. The equivalent wind observation errors estimated and presented here for asm_uv and asm_sd are more focused on making a fair comparison of the assimilation scheme.

The BKG-QC in asm_sd needs to be further studied. It is likely that the innovation threshold of 90° for *dir* observations is too strict to retain most useful observations. For example, in the precipitation case presented, some good *dir* observations with an innovation score above 90° were observed in the vicinity of the frontal system when a phase difference exists between the observations and the background. Further investigations of the estimation and tuning of *spd* and *dir* observation errors for all wind observation types and the corresponding BKG-QC scheme should be conducted.

Additionally, although the mass variables in the surface dataset are also assimilated along with the wind observations, the proportion of wind-to-mass observations in this study is skewed towards the impact of wind observations versus what would be expected in an operational configuration.

Another interesting topic exists regarding BKG-QC of wind observations in asm_uv that deserves investigation. As discussed, the BKG-QC in asm_uv is conducted for the *u* and *v* components separately, which means that either *u* or *v* could be rejected or assimilated without the other. However, it seems unreasonable to assimilate the other variable when its respective component is rejected because the *u* and *v* components are calculated from a single observational pair of *spd* and *dir,* and the observation error in either *spd* or *dir* can simultaneously affect the errors in both *u* and *v*. Is alone *u* or *v* able to usefully contribute to wind vector analyses when one of them is rejected? Or is it more helpful to reject both of them when one of them fails QC? The question is not addressed here, but is worthy of further discussion.

6. Acknowledgements

References

Andersson, E., Haseler, J., Undén, P., Courtier, P., Kelly, G. and co-authors. 1998. The ECMWF implementation of three-dimensional variational assimilation (3D-Var). III: experimental results. *Q. J. Roy. Meteorol. Soc.* **124**, 1831–1860.

Barker, D., Huang, X.-Y., Liu, Z., Auligné, T., Zhang, X. and co-authors. 2012. The weather research and forecasting (WRF)

model's community variational/ensemble data assimilation system: WRFDA. *Bull. Am. Meteorol. Soc*. **93**, 831–843.

Benjamin, S. G., Schwartz, B. E. and Cole, R. E. 1999. Accuracy of ACARS wind and temperature observations determined by collocation. *Weather Forecast*. **14**, 1032–1038.

Drüe, C., Frey, W., Hoff, A. and Hauf, T. 2008. Aircraft type-specific errors in AMDAR weather reports from commercial aircraft. *Q. J. Roy. Meteorol. Soc*. **134**, 229–239.

Gao, F., Zhang, X. Y., Jacobs, N. A., Huang, X.-Y., Zhang, X. and co-authors. 2012. Estimation of TAMDAR observational error and assimilation experiments. *Weather Forecast*. **27**, 856–877.

Gustafsson, N., Berre, L., Hornquist, S., Huang, X.-Y., Lindskog, M. and co-authors. 2001. Three-dimensional variational data assimilation for a limited area model. *Tellus A*. **53**, 425–446.

Hollingsworth, A. and Lönnberg, P. 1986. The statistical structure of short-range forecast errors as determined from radiosonde data. Part I: the wind field. *Tellus A*. **38A**, 111–136.

Huang, X-Y., Gao, F., Jacobs, N. A. and Wang, H. 2013. Assimilation of wind speed and direction observations: a new formulation and results from idealized experiments. *Tellus A*. **65**, 19936. DOI: 10.3402/tellusa.v65i0.19936.

Huang, X.-Y., Xiao, Q., Barker, D., Zhang, X., Michalakes, J. and co-authors. 2009. Four-dimensional variational data assimilation for WRF: formulation and preliminary results. *Mon. Weather Rev*. **137**, 299–314.

Jarvinen, H., Andersson, E. and Bouttier, F. 1999. Variational assimilation of time sequences of surface observations with serially correlated errors. *Tellus A*. **51**, 469–488.

Kalnay, E., Kanamitsu, M., Kistler, R., Collins, W., Deaven, D. and co-authors. 1996. The NCEP/NCAR 40-year reanalysis project. *Bull. Am. Meteorol. Soc*. **77**, 437–471.

Le Dimet, F. and Talagrand, O. 1986. Variational algorithms for analysis and assimilation of meteorological observations: theoretical aspects. *Tellus A*. **38A**, 97–110.

Lin, Y. and Mitchell, K. E. 2005. The NCEP stage II/IV hourly precipitation analyses: development and applications. Preprints, In: *19th Conference on Hydrology*, San Diego, CA, American Meteorological Society, CD-ROM, 1.2.

Lindskog, M., Gustafsson, N., Navascués, B., Mogensen, K. S., Huang, X.-Y. and co-authors. 2001. Three-dimensional variational data assimilation for a limited area model. Part II: Observation handling and assimilation experiments. *Tellus A*. **53A**, 447–468.

Moninger, W. R., Benjamin, S. G., Jamison, B. D., Schlatter, T. W., Smith, T. L. and co-authors, 2010. Evaluation of regional aircraft observations using TAMDAR. *Weather Forecast*. **25**, 627–645.

Painting, D. J. 2003. *AMDAR reference manual*. WMO, 84 pp. Online at: http://amdar.wmo.int/Publications/AMDAR_Reference_Manual_2003.pdf

Parrish, D. F. and Derber, J. C. 1992. The National Meteorological Center's Spectral Statistical Interpolation analysis system. *Mon. Weather Rev*. **120**, 1747–1763.

Plant, W. J. 2000. Effects of wind variability on scatterometry at low wind speeds. *J. Geophys. Res*. **105**, 16899–16910.

Skamarock, W., Klemp, J., Dudhia, J., Gill, D., Barker, D. and co-authors. 2008. *A Description of the Advanced Research WRF Version 3*. NCAR Tech. Note, 2008. NCAR/TN–475 + STR. pp. 1–113.

Velden, C. S., Olander, T. L. and Wanzong, S. 1998. The impact of multispectral GOES-8 wind information on Atlantic tropical cyclone track forecasts in 1995. Part I: Dataset methodology, description, and case analysis. *Mon. Weather Rev*. **126**, 1202–1218.

Wu, W. S., Purser, R. J. and Parrish, D. F. 2002. Three-dimensional variational analysis with spatially inhomogeneous covariances. *Mon. Weather Rev*. **130**, 2905–2916.